Editors' Suggestion

Partially coherent vortex beams of arbitrary radial order and a van Cittert–Zernike theorem for vortices

Yongtao Zhang,[1,2] Yangjian Cai,[3,4] and Greg Gbur[2,*]

[1]*College of Physics and Information Engineering, Minnan Normal University, Zhangzhou 363000, China*
[2]*Department of Physics and Optical Science, University of North Carolina at Charlotte, Charlotte, North Carolina 28277, USA*
[3]*Shandong Provincial Engineering and Technical Center of Light Manipulations & Shandong Provincial Key Laboratory of Optics and Photonic Device, School of Physics and Electronics, Shandong Normal University, Jinan 250014, China*
[4]*School of Physical Science and Technology, Soochow University, Suzhou 215006, China*

(Received 23 May 2019; revised manuscript received 26 February 2020; accepted 2 March 2020; published 13 April 2020)

We theoretically define a complete class of partially coherent vortex beams of any radial and azimuthal order and characterize the behavior of their phase singularities and orbital angular momentum. These beams are shown to exhibit a coherence vortex supplement to the van Cittert–Zernike theorem, in which the vortex structure of the random beam reconstitutes upon propagation. This full characterization of a class of partially coherent Laguerre-Gauss beams of any order may find application in free-space optical communication, among other uses.

DOI: 10.1103/PhysRevA.101.043812

I. INTRODUCTION

The study of vortex structures in optical fields, and other types of wave-field singularities, has become a significant area of investigation in modern optics, termed singular optics [1–3]. Spatially coherent beams carrying optical vortices, which are called vortex beams, have attracted much interest due to their potential usefulness in diverse areas such as coronagraphy [4], coherence filtering [5], and free-space optical communication [6]. Since Allen *et al.* found that Laguerre-Gauss (LG) beams, possessing a phase vortex core, consequently carry a well-defined orbital angular momentum (OAM) [7], vortex beams have also been employed in optical trapping and rotation [8] and the design of light-driven machines [9].

In a seemingly unrelated development, beams which are partially coherent have also been shown to be advantageous in many applications, including free-space optical communication [10], particle trapping [11], and atom cooling [12]. The overlap between the applications of vortices and the applications of partial coherence makes it quite attractive to consider their synthesis, namely, vortex structures in partially coherent beams. When dealing with such a situation, however, the phase of the field is not well defined, as it is a random variable in space and time. Instead, researchers have investigated analogous phase singularities in the two-point correlation function of partially coherent beams; the typical forms of such singularities are known as correlation singularities or coherence vortices [13–16].

For partially coherent beams carrying vortex structures, which are now referred to as partially coherent vortex beams (PCVBs), it is known that optical vortices evolve into coherence vortices when the spatial coherence is decreased [17]. Because coherence vortices are robust under such a decrease, they may prove to be useful structures to carry information in free-space optical communication. Furthermore, it was recently found that PCVBs have a more diverse set of OAM characteristics than their spatially coherent vortex counterparts, making them interesting physical objects of study in their own right [18]. Simple classes of PCVBs may exhibit an OAM density analogous to a fluid-body rotator, a rigid-body rotator, or a Rankine vortex—a mixture of the two former classes [19].

Though there are now a number of publications on the properties of PCVBs, most of the research has been restricted to LG beams of low azimuthal order. This work began with the introduction of a "beam wander" model for a partially coherent vortex beam of radial order $n = 0$ and azimuthal order $m = 1$ in the waist plane [17] and continued to the study of such beams upon propagation [16]. Quite recently, this work was extended to the analysis of PCVBs of radial order $n = 0$ and any azimuthal order m [20], introducing a whole class of beams with different topological and OAM characteristics. But the radial order of the beam will also affect these characteristics, and it has been shown that radial orders may also be used for multiplexing and demultiplexing of signals [21]. It is therefore of interest to study the behavior of PCVBs of any radial and azimuthal order. To date, only one other paper has investigated such beams in detail; however, their model of a PCVB could only be analyzed computationally [22].

In this paper, we determine a generalized analytic solution for partially coherent Laguerre-Gauss beams of any radial order, of any azimuthal order, and at any propagation distance. The OAM properties of these beams are analyzed and the behavior of coherence vortices with different degrees of coherence and different radial and azimuthal orders is studied. The use of an analytic solution allows us to examine in detail

*gjgbur@uncc.edu

the origins of any unusual topological features present in the beam, and we observe an unexpected reconstruction of the coherent vortex structure upon propagation, which we consider a vortex supplement to the van Cittert–Zernike theorem. These results complete the characterization of analytic PCVBs and they open the door for their use in applications such as free-space optical communications.

II. DERIVATION OF RADIAL-ORDER PCVBs

Our derivation of PCVBs with any radial order follows the same general strategy applied in our previous work [20]; here we outline this calculation, highlighting any new considerations that arise when radial order is included.

To characterize the coherence properties, we work in the frequency domain and calculate the cross-spectral density function $W(\mathbf{r}_1, \mathbf{r}_2, z)$ of the beams, which can be written as an average over an ensemble of monochromatic realizations of the field $U(\mathbf{r}, z)$ in the form

$$W(\mathbf{r}_1, \mathbf{r}_2, z) = \langle \tilde{U}(\mathbf{r}_1, z) U(\mathbf{r}_2, z) \rangle, \tag{1}$$

where $\langle \cdots \rangle$ represents the ensemble average and a tilde is used to represent complex conjugation throughout the paper.

In the modeling of a partially coherent vortex beam, we have great freedom in the choice of ensemble, a point which we find important in Sec. IV. Here we continue to use the venerable "beam wander" model [17] introduced in 2004, in which every member of the ensemble is a coherent beam but with a random central axis position $\mathbf{r}_0$. We may then write

$$W(\mathbf{r}_1, \mathbf{r}_2, z) = \int P(\mathbf{r}_0) \tilde{U}(\mathbf{r}_1 - \mathbf{r}_0, z) U(\mathbf{r}_2 - \mathbf{r}_0, z) d^2 r_0, \tag{2}$$

where $P(\mathbf{r}_0)$ is the probability density of the axis position, which we take to be of Gaussian form,

$$P(\mathbf{r}_0) = \frac{1}{\pi \delta^2} \exp\left(-\frac{r_0^2}{\delta^2}\right), \tag{3}$$

with $r_0 = \sqrt{x_0^2 + y_0^2}$ the transverse radial position of the axis and δ the variance of the beam wander. In the limit $\delta \to 0$, the beam axis position is fixed and the beam is spatially coherent; an increase in δ results in a decrease in spatial coherence.

In Ref. [20], the foundational member of the ensemble was taken to be a Laguerre-Gauss beam of radial order $n = 0$ and arbitrary azimuthal order m. We now generalize this and consider a foundational member of arbitrary radial order n and arbitrary azimuthal order m, with $m \geqslant 0$ for convenience. The field $U_{nm}(\mathbf{r}, z)$ may be written in cylindrical coordinates (r, ϕ, z) in the form [3, chap. 2]

$$U_{nm}(\mathbf{r}, z) = C(z) L_n^m\left[\frac{2r^2}{w^2(z)}\right] \exp\left[-\frac{r^2}{\sigma^2(z)}\right] r^m \times \exp[im\phi] \exp[-i\Phi(z)(2n + m + 1)], \tag{4}$$

where L_n^m is an associated Laguerre function of order n and m. Other parameters are defined in the usual way for LG beams, with $w(z)$ representing the beam width, $R(z)$ representing the wave-front curvature, $\Phi(z)$ representing the Gouy phase shift, and $\sigma(z)$ a complex propagation constant; these formulas are all given in Ref. [20]. We define w_0 as the beam waist width and $z_0 = \pi w_0^2/\lambda$ is consequently the Rayleigh range of the beam, with λ the wavelength. The quantity $C(z)$ is a normalization function, given by

$$C(z) = \sqrt{\frac{2n!}{\pi w^2(z)(n+m)!}} \left(\frac{\sqrt{2}}{w(z)}\right)^m. \tag{5}$$

It is noteworthy that the vortex is characterized by the term $r^m \exp[im\phi] = (x + iy)^m$; this is the functional form of a vortex we will look for in our final results.

We may substitute from Eqs. (4) and (3) into Eq. (2). The resulting integrand contains terms of Gaussian form and polynomials of $x_0 \pm iy_0$, which can be readily integrated analytically. The exception is the associated Laguerre functions, which only appear when we have $n > 0$. We take the direct approach of writing them in their power-series form, namely,

$$L_n^m(x) = \sum_{k=0}^{n} \frac{[-1]^k}{k!} \binom{n+m}{n-k} x^k, \tag{6}$$

where the parentheses indicate a binomial coefficient. The argument of the associated Laguerre functions in Eq. (4) is proportional to $|\mathbf{r} - \mathbf{r}_0|^2$, which may be written as

$$|(x - x_0) + i(y - y_0)|^2 = |(x + iy) - (x_0 + iy_0)|^2. \tag{7}$$

Therefore the Laguerre functions may also be written as polynomials of $x_0 \pm iy_0$.

Upon further substituting this associated Laguerre representation into Eq. (2), everything may be evaluated analytically, albeit with significant effort. The radial and azimuthal components of $\mathbf{r}_0$ may be integrated separately, as done in Ref. [20]. The result is given by the lengthy expression

$$\begin{aligned} W(\mathbf{r}_1, \mathbf{r}_2, z) = \pi D(\mathbf{r}_1, \mathbf{r}_2, z) &\sum_{p=0}^{n} \sum_{q=0}^{n} \sum_{k_1=0}^{m+p} \sum_{l_1=0}^{p} \sum_{k_2=0}^{q} \sum_{l_2=0}^{m+q} \\ &\binom{n+m}{n-p} \binom{n+m}{n-q} \binom{m+p}{k_1} \binom{m+q}{l_2} \binom{p}{l_1} \binom{q}{k_2} \\ &\times (-1)^{p+q+2k_1+2k_2} \frac{1}{p!q!} \left(\frac{2}{w^2(z)}\right)^{p+q} \frac{\Gamma(k_1 + k_2 + 1)}{A^{2m+2p+2q-k_1-k_2+1}} \\ &\times \left[\frac{1}{\alpha^2}(x_1 - iy_1) - \frac{1}{\sigma^2}(x_2 - iy_2)\right]^{m+p-k_1} \\ &\times \left[\frac{1}{\alpha^2}(x_1 + iy_1) - \frac{1}{\sigma^2}(x_2 + iy_2)\right]^{p-l_1} \\ &\times \left[\frac{1}{\tilde{\alpha}^2}(x_2 - iy_2) - \frac{1}{\tilde{\sigma}^2}(x_1 - iy_1)\right]^{q-k_2} \\ &\times \left[\frac{1}{\tilde{\alpha}^2}(x_2 + iy_2) - \frac{1}{\tilde{\sigma}^2}(x_1 + iy_1)\right]^{m+q-l_2}. \end{aligned} \tag{8}$$

This equation is an analytic expression for the entire class of PCVBs of any radial order n, of any azimuthal order m, and at any propagation distance z. It is the main result of this paper. This expression has been derived for positive azimuthal order m, but the negative-order result can be derived by switching the sign of the imaginary part of each term of the form $(x + iy)$ or $(x - iy)$.

In Eq. (8) we have introduced the parameters

$$A = \frac{1}{\tilde{\sigma}^2} + \frac{1}{\sigma^2} + \frac{1}{\delta^2}, \quad \frac{1}{\alpha^2} = \frac{1}{\sigma^2} + \frac{1}{\delta^2}, \tag{9}$$

and it is noteworthy that the obvious dependence of A, σ, and α on z has been suppressed for brevity.

The origins of the summations in Eq. (8) are worth explaining. The sums $\sum_{p=0}^{n}\sum_{q=0}^{n}$ come from the expansion of the two associated Laguerre functions. The remaining four come from the method of evaluating the integral: each term of the form $(x_k - x_0) \pm i(y_k - y_0)$, where $k = 1, 2$, must be expanded in a binomial expansion to extract the x_0, y_0 terms. The associated Laguerre function arguments contain $(x_k - x_0)^2 + (y_k - y_0)^2$, and each requires two binomial expansions; when $n = 0$, the Laguerre functions are constants and only two sums are needed. The sums have the additional constraint that only terms with $l_1 + l_2 = k_1 + k_2$ are nonzero.

The term $D(\mathbf{r}_1, \mathbf{r}_2, z)$ is of the form

$$D(\mathbf{r}_1, \mathbf{r}_2, z) = \frac{|C|^2}{\pi\delta^2} \exp\left[-\frac{r_1^2}{A\tilde{\sigma}^2\delta^2}\right] \exp\left[-\frac{r_2^2}{A\sigma^2\delta^2}\right] \times \exp\left[-\frac{(\mathbf{r}_1 - \mathbf{r}_2)^2}{A|\sigma|^4}\right], \tag{10}$$

which is the expression of a Gaussian Schell-model beam [23]. The entire class of PCVBs may therefore be said to have a global correlation length σ_μ of

$$\sigma_\mu^2 = A|\sigma|^4 = w^2 \frac{2 + \frac{w^2}{\delta^2}}{1 + \frac{k^2 w^4}{4R^2}}. \tag{11}$$

In this expression, $k = 2\pi/\lambda$ is the wave number.

For $n = 0$, Eq. (8) reduces to the form of Eq. (27) of [20], which was the derivation of PCVBs of any azimuthal order and radial order $n = 0$. Equation (8) generalizes that previous result and provides us with a closed-form solution for PCVBs of any radial order n and any azimuthal order m, at any propagation distance. We may now investigate what effect the radial order has on the behavior of PCVBs.

III. ORBITAL ANGULAR MOMENTUM

Most free-space optical communication schemes sort modes by their orbital angular momentum. We therefore begin our analysis of our radial-order PCVBs by considering their OAM properties.

In general, the angular momentum of light is a combination of spin (polarization) and orbital (phase) angular momentum and must be treated vectorially. Here we consider a paraxial scalar partially coherent beam, which on average has no spin angular momentum. The OAM flux density $M_d(\mathbf{r}, z)$ of such a field along the z axis can be expressed as [24]

$$M_d(\mathbf{r}, z) = -\frac{\epsilon_0}{k}\mathrm{Im}\{y_1 \partial_{x_2} W(\mathbf{r}_1, \mathbf{r}_2, z) - x_1 \partial_{y_2} W(\mathbf{r}_1, \mathbf{r}_2, z)\}_{\mathbf{r}_1 = \mathbf{r}_2}, \tag{12}$$

where ∂_{x_2} and ∂_{y_2} represent the partial derivatives with respect to x_2 and y_2, respectively. Upon substitution from Eq. (8) into Eq. (12), we have

$$M_d(\mathbf{r}, z) = \frac{\epsilon_0}{k}\frac{|C|^2}{\delta^2} \exp\left[-\frac{2r^2}{\beta w^2(z)}\right] \sum_{p=0}^{n}\sum_{q=0}^{n}\sum_{k_1=0}^{m+p}\sum_{l_1=0}^{p}\sum_{k_2=0}^{q}\sum_{l_2=0}^{m+q} \binom{n+m}{n-p}\binom{n+m}{n-q}\binom{m+p}{k_1}\binom{m+q}{l_2}\binom{p}{l_1}\binom{q}{k_2} \times (-1)^{p+q+2k_1+2k_2} \frac{1}{p!q!}\left(\frac{2}{w^2(z)}\right)^{p+q} \frac{\Gamma(k_1+k_2+1)}{A^{k_1+k_2+1}} (m + l_1 - k_1) r^{2m+2p+2q-2k_1-2k_2+2} \left(\frac{1}{\beta}\right)^{2m+2p+2q-2k_1-2k_2-1}, \tag{13}$$

with

$$\beta \equiv \left(1 + \frac{2\delta^2}{w^2(z)}\right). \tag{14}$$

This complicated expression for the OAM flux density $M_d(\mathbf{r}, z)$ describes the spatial distribution of OAM within the cross section of a beam. However, this expression alone obscures the physics, because this flux depends not only on the strength of circulation of the phase at a location, but also on the intensity of the beam at that location. To isolate the circulation, we may consider a normalized OAM flux density $m_d(\mathbf{r}, z)$, which represents the average OAM flux density per photon,

$$m_d(\mathbf{r}, z) = \frac{\hbar\omega M_d(\mathbf{r}, z)}{S(\mathbf{r}, z)}, \tag{15}$$

where $S(\mathbf{r}, z)$ is the z component of the Poynting vector. This quantity describes the average OAM that would be measured for a photon at that particular point in space. The Poynting vector expression is given by

$$\begin{aligned} S(\mathbf{r}, z) &= \frac{k}{\mu_0\omega} W(\mathbf{r}, \mathbf{r}, z) \\ &= \frac{k}{\mu_0\omega}\frac{|C|^2}{\delta^2} \exp\left[-\frac{2r^2}{\beta w^2(z)}\right] \sum_{p=0}^{n}\sum_{q=0}^{n}\sum_{k_1=0}^{m+p}\sum_{l_1=0}^{p}\sum_{k_2=0}^{q}\sum_{l_2=0}^{m+q} \binom{n+m}{n-p}\binom{n+m}{n-q}\binom{m+p}{k_1}\binom{m+q}{l_2}\binom{p}{l_1}\binom{q}{k_2} \\ &\quad \times (-1)^{p+q+2k_1+2k_2} \frac{1}{p!q!}\left(\frac{2}{w^2(z)}\right)^{p+q} \frac{\Gamma(k_1+k_2+1)}{A^{k_1+k_2+1}} r^{2m+2p+2q-2k_1-2k_2} \left(\frac{1}{\beta}\right)^{2m+2p+2q-2k_1-2k_2}. \end{aligned} \tag{16}$$

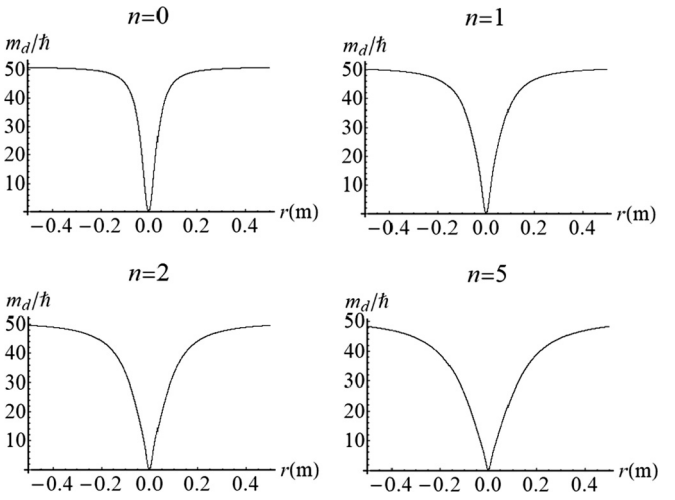

FIG. 1. Distributions of the normalized OAM flux density $m_d/\hbar$ at $z = 0$ for different radial orders n. Here we have taken $w_0 = 1$ mm, $\delta = 5$ mm, and $m = 1$.

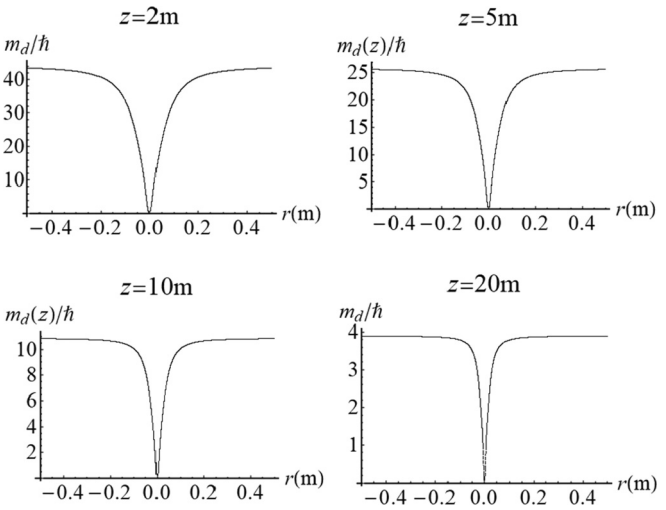

FIG. 2. Distributions of the normalized OAM flux density $m_d/\hbar$ at different propagation distances with $w_0 = 1$ mm, $\delta = 5$ mm, $m = 1$, and $n = 1$.

A complementary quantity is the total average OAM per photon m_t of the PCVBs, which is given by

$$m_t = \frac{\hbar\omega \int M_d(\mathbf{r}, z) d^2 r}{\int S(\mathbf{r}, z) d^2 r} = m\hbar. \tag{17}$$

It is readily found that m_t is simply proportional to the topological charge m of the underlying vortex beam and independent of the radial order n; this is not surprising, as our ensemble is constructed entirely from pure LG beams with topological charge m and OAM $m\hbar$, and the OAM of LG beams has been shown to be intrinsic, i.e., independent of the axis of measurement [25].

The radial order, however, will affect the distribution of OAM in the beam, as indicated by the normalized OAM flux density. Figure 1 shows the normalized OAM flux density of PCVBs with a different radial order; as the beams are rotationally symmetric, only a cross section of this density is shown.

It can be seen that the beams in general act like Rankine vortices, with a quadratic radial dependence near the core and a constant value in the outskirts, analogous to rigid-body rotation and fluid-body rotation, respectively. This follows directly from the asymptotic behavior of Eqs. (13) and (16). It can be seen that a higher radial order corresponds to a wider quadratic region in the beam, i.e., a more Rankine-like behavior. This indicates that the radial order may be used as well as the spatial coherence to adjust the distribution of the OAM within a beam. For PCVBs, in contrast to coherent vortex beams, the radial order provides an extra degree of freedom to control OAM properties.

What is the origin of this increased width for $n > 0$? For $n = 0$, the Rankine vortex behavior may be interpreted as arising from the random motion of the vortex core, which results in rapid changes in phase near the central axis of the beam and on average disrupts the helicity of the phase. For $n > 0$, the zero rings, across which the phase jumps by π, also contribute to this rapid change of phase, resulting in a broader Rankine region.

Figure 2 shows the distribution of the normalized OAM flux density at different propagation distances. It can be seen that the beam looks increasingly like a pure fluidlike rotator as z increases. As a coherent vortex beam has a pure fluidlike OAM flux density, this observation suggests that our beams appear to grow more coherent upon propagation, at least with respect to their OAM behavior. We elaborate on this in the next section.

For large values of r, the normalized OAM flux density takes on the approximate form

$$m_d \approx m\hbar\left(1 + \frac{2\delta^2}{w_0^2(1 + z^2/z_0^2)}\right), \tag{18}$$

in agreement with Fig. 2, which shows that the value of m_d at the beam outskirts decreases with increasing propagation distance. It is also noteworthy that this asymptotic value of m_d is independent of the radial order n.

IV. TOPOLOGICAL PROPERTIES

A coherent LG vortex beam has a discrete topological charge equal to its azimuthal index $\pm m$, which represents the number of multiples of 2π the phase changes by as one takes a counterclockwise circuit around the beam axis. Because it is a discrete and conserved quantity, the topological charge has also been considered as an alternative means to encode information in a beam for free-space optical communications. In fact, it has been shown that the OAM and topological charge are related, but not equivalent, properties of a wave field [26]. In considering the use of topological charge for communications, it is therefore of interest to understand how the topological structure changes with a change in coherence.

As noted in Sec. I, vortices of a coherent optical field evolve into vortices of the cross-spectral density as the spatial coherence is decreased. As the cross-spectral density is a two-point correlation function, the complete structure of the singularity is quite complicated [27], and investigators have typically studied projections of the cross-spectral density onto

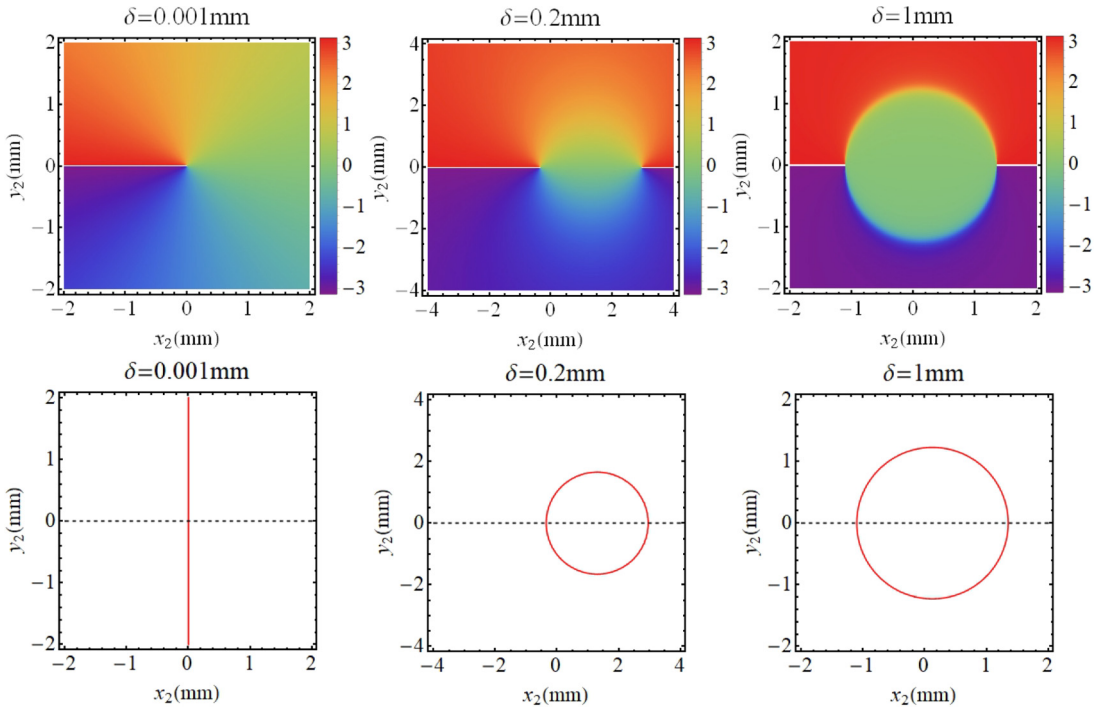

FIG. 3. Phase and corresponding zeros of real and imaginary parts of the cross-spectral density for different values of the coherence parameter δ, with $n = 0$ and $z = 0$. The top row shows color contours, while the bottom row shows only the solutions of Eq. (21). In all images, $\mathbf{r}_1 = (0.1\text{ mm}, 0.0\text{ mm})$, $m = 1$, $w_0 = 1$ mm, and $\lambda = 632.8$ nm.

a lower-dimensional space. When one observation point, say $\mathbf{r}_1$, is fixed, the cross-spectral density exhibits coherence vortices with respect to the other point.

The analytic form of Eq. (8) allows us to clearly see how the behavior of coherence vortices depends on the radial order n of the beam. A careful examination of the highest-order terms of the sum indicates that it is an $(m + 2n)$th-order polynomial in $x_2 + iy_2$ and an $(m + 2n)$th polynomial in $x_2 - iy_2$, or $(m + 2n)$ vortices of charge $+1$ and $(m + 2n)$ vortices of charge -1. The net topological charge, considered over the entire infinite cross section of the beam, is 0. For $n = 0$ and $m > 0$, it has been shown [20] that a decrease in coherence results in the original vortex m breaking into m vortices of charge $+1$ and m vortices of charge -1 approaching from ∞. We must now consider the origin of the additional zeros when $n > 0$.

Correlation singularities exist at pairs of points $\mathbf{r}_1$ and $\mathbf{r}_2$ for which the spectral degree of coherence $\mu(\mathbf{r}_1, \mathbf{r}_2, z)$ of the field vanishes, i.e.,

$$\mu(\mathbf{r}_1, \mathbf{r}_2, z) = \frac{W(\mathbf{r}_1, \mathbf{r}_2, z)}{\sqrt{S(\mathbf{r}_1, z)S(\mathbf{r}_2, z)}} = 0, \tag{19}$$

where $S(\mathbf{r}, z)$ is the spectral density of the field, defined as

$$S(\mathbf{r}, z) = W(\mathbf{r}, \mathbf{r}, z). \tag{20}$$

The spectral density is typically not equal to 0 for partially coherent fields [28]; therefore the zeros of the spectral degree of coherence will be the only zeros of the cross-spectral density, and we may work with this mathematically simpler cross-spectral density in the following simulations, with zeros at locations such that the expressions

$$\text{Re}[W(\mathbf{r}_1, \mathbf{r}_2, z)] = 0, \quad \text{Im}[W(\mathbf{r}_1, \mathbf{r}_2, z)] = 0 \tag{21}$$

are simultaneously satisfied.

For a fixed value of $\mathbf{r}_1$ and z, Eq. (21) represents a system of equations with two constraints and two degrees of freedom, x_2 and y_2; the solutions are therefore points in any transverse plane of the beam. Going forward, we restrict our attention to the case $\mathbf{r}_1 = (0.1\text{ mm}, 0.0\text{ mm})$ and take $m = 1$, $w_0 = 1$ mm, and $\lambda = 632.8$ nm.

For future comparison, we first review the case $n = 0$ in Fig. 3, as the spatial coherence of the field is decreased. It is shown that in the coherent limit, there exists a vortex core with topological charge $m = 1$ at the center, which can be regarded as the phase vortex of the coherent LG beam. As the coherence decreases, a new singularity with topological charge $m = -1$ comes in from the point at ∞. And a further decrease in the coherence will result in the movement of the original vortex away from the center. The result is consistent with Fig. 4 in [17]. It is noteworthy that the singularities lie along the horizontal, a consequence of our choice of the location of the fixed point $\mathbf{r}_1$, which breaks the rotational symmetry of the cross-spectral density.

It can be difficult to identify singularities in colored phase plots, especially when there are many closely packed together. For this reason, we often resort to plotting only the solutions of Eq. (21); the intersection of the zeros of the real and imaginary parts of $W(\mathbf{r}_1, \mathbf{r}_2, z)$ presents a clear way to identify coherence vortices, as shown in the bottom row in Fig. 3. Any location where a solid red line and a dashed line intersect represents the presence of a vortex.

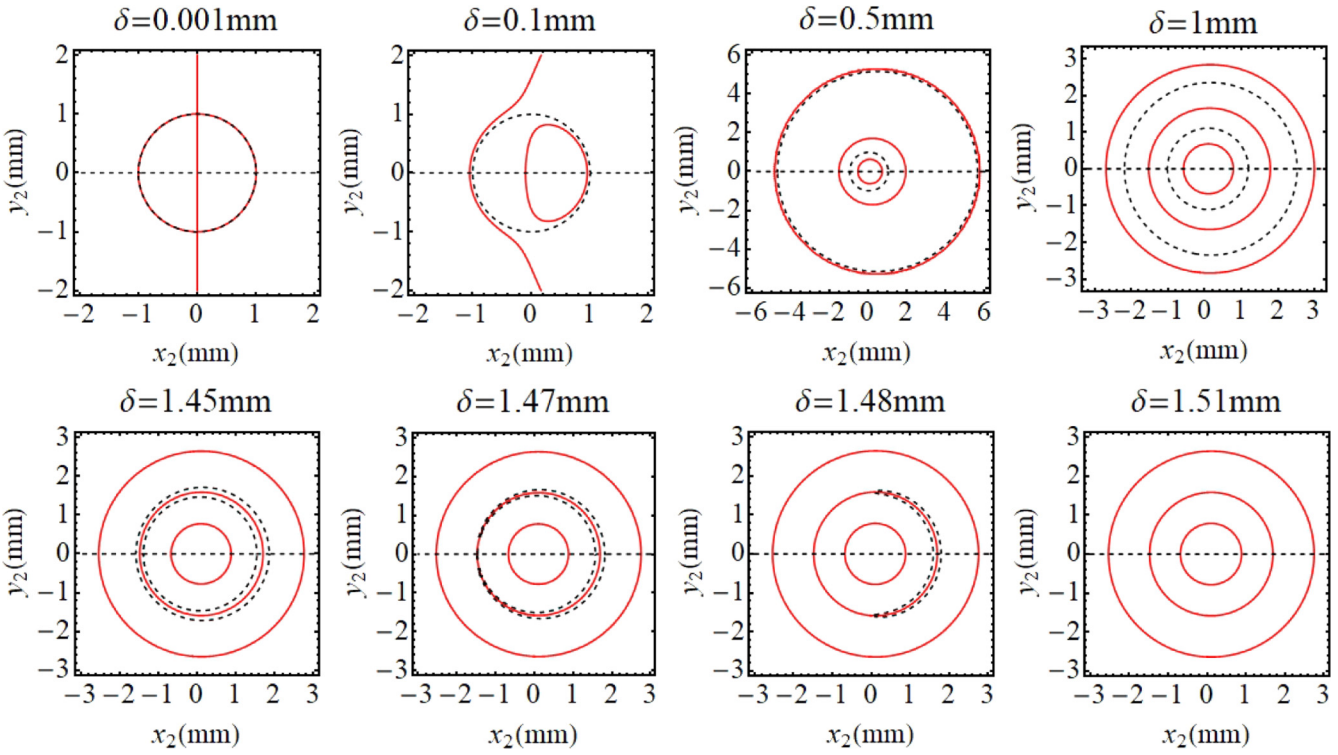

FIG. 4. Zeros of real and imaginary parts of the cross-spectral density for different values of the coherence parameter δ, with $n = 1$ and $z = 0$. In all images, $\mathbf{r}_1 = (0.1\text{ mm}, 0.0\text{ mm})$, $m = 1$, $w_0 = 1$ mm, and $\lambda = 632.8$ nm.

We now consider the effect of the radial order on the behavior of correlation singularities. Figure 4 illustrates their evolution for $n = 1$ as δ is increased. In the coherent limit, there exists a vortex core surrounded by a single zero ring, which is the coincidence of circles with $\mathrm{Re}[W] = 0$ and $\mathrm{Im}[W] = 0$. As the beam wander is increased to $\delta = 0.1$ mm, the immediate effect is that the zero ring breaks up, resulting in a new pair of first-order vortices of opposite charge. This is the result of the lines with $\mathrm{Re}[W] = 0$ and $\mathrm{Im}[W] = 0$ no longer perfectly overlapping, but possessing two intersection points.

As the wander is increased further, to $\delta = 0.5$ mm, we find that two things have happened. First, a second vortex of opposite sign has come in from ∞, as in the $n = 0$ case, resulting in two pairs of first-order vortices of opposite sign near the origin (two vortices at $x_2 \approx \pm 1$ mm and two at $x_2 \approx \pm 2$ mm). Second, a new zero ring with a large radius has appeared; this is apparently analogous to the appearance of the second vortex from ∞ in the $n = 0$ case, but for zero rings. Finally, that second zero ring also breaks up, resulting in yet another pair of vortices of opposite sign. As δ is increased even more, the arrangement of singularities stabilizes, resulting in three positive and three negative first-order vortices along the horizontal, as in the case $\delta = 1.51$ mm. This is in agreement with our observations from Eq. (8), which indicate that there should be $(m + 2n)$ positive vortices and $(m + 2n)$ negative vortices in the partially coherent field.

In summary, a decrease in coherence causes an mth-order vortex to break up and m vortices of opposite handedness to manifest from ∞. Each zero ring also has a complementary ring appear, and each ring breaks into a pair of vortices of opposite handedness.

A similar evolution happens for beams of larger radial order n, as illustrated in Fig. 5. In this case, the two zero rings immediately break into pairs of positive and negative vortices, and two new zero rings of large radius appear. For sufficiently low coherence, the result is five positive and five negative vortices along the horizontal axis, as $m + 2n = 5$.

These results indicate one significant difficulty in using beams with $n > 0$ to carry information in vortices. As soon as the spatial coherence is decreased, the rings will decompose into vortex pairs. Though the net change in topological charge is 0, there is always the possibility that one member of a pair will fall outside of the detector aperture, resulting in an effective change in measured topological charge, as happens to coherent vortex beams in atmospheric propagation [29].

We next consider the effect of propagation on the topological features of the beam. Figure 6 shows the evolution of the phase structure of a partially coherent beam over a 100-m propagation range. Though the field starts out with the vortex structure characteristic of a low-coherence source, as it evolves it takes on the very simple form of a coherent vortex beam; compare with the left column in Fig. 3.

It can be shown that the same effect occurs for PCVBs of any radial and azimuthal order; in Fig. 7, we examine the evolution of a beam of order $n = 2$. Both the zero rings and the central vortex core self-reconstruct upon propagation, even though the source field was highly random.

This result appears to be a topological version of the classic van Cittert–Zernike theorem of optical coherence theory, in

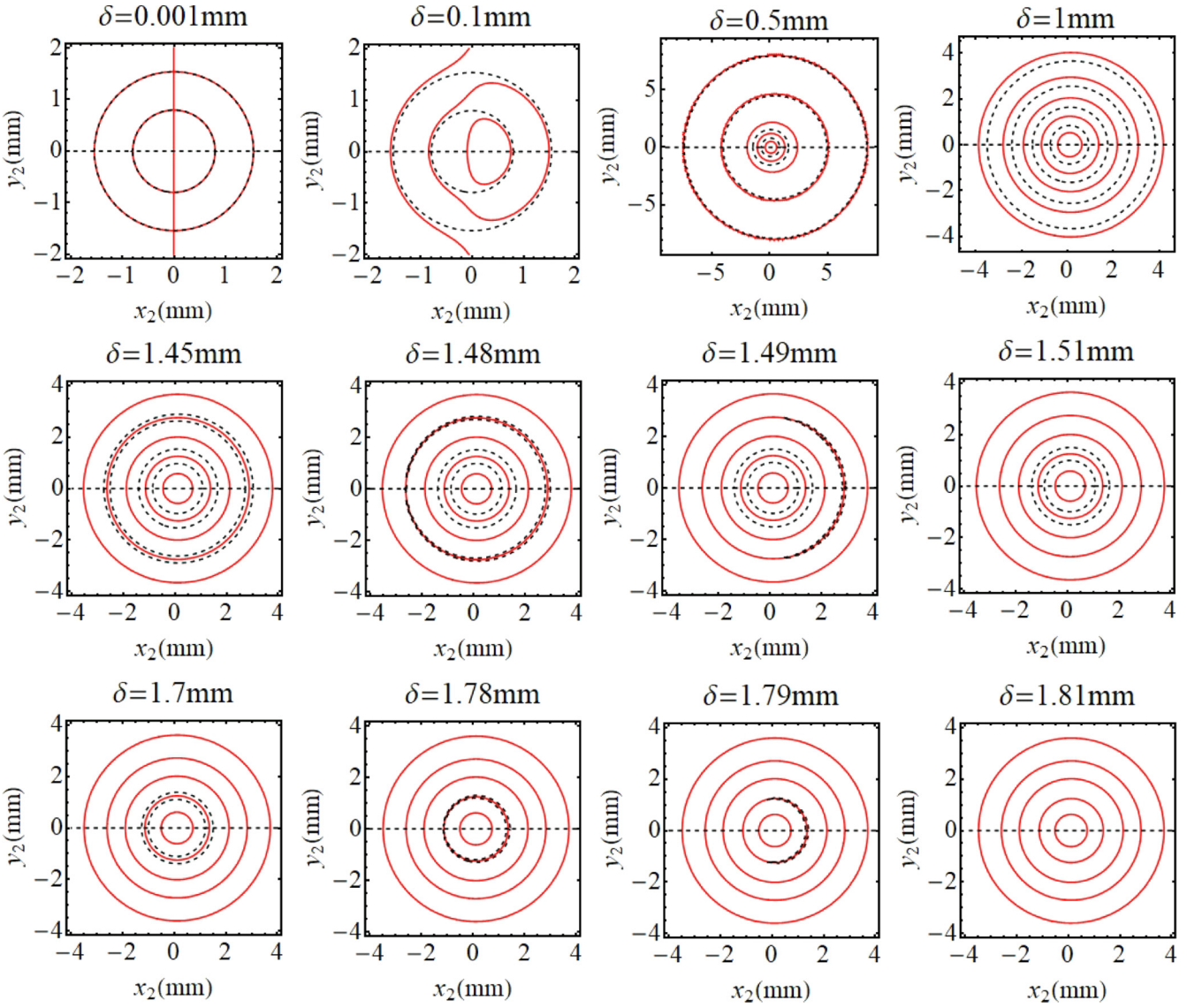

FIG. 5. Zeros of real and imaginary parts of the cross-spectral density for different values of the coherence parameter δ, with $n = 2$ and $z = 0$. In all images, $\mathbf{r}_1 = (0.1\text{ mm}, 0.0\text{ mm})$, $m = 1$, $w_0 = 1$ mm, and $\lambda = 632.8$ nm.

which it was shown that the light from an incoherent source becomes increasingly more coherent as it propagates [23]. In this case, we see that not only does the spatial coherence increase upon propagation, but the topological properties of the field reconstruct themselves. It is well known that vortex beams can "self-heal" after being distorted by a deterministic obstacle [30], and these figures suggest that this self-healing can also apply when a vortex beam is randomly distorted.

This result is surprising, in large part because PCVBs have been studied for some time [31], but this topological reconstruction has evidently not been observed before, though there is a hint of it in Fig. 3 in [32]. The discrepancy evidently arises because the evolution of the topological features depends on the manner in which it is randomized. Most theoretical and experimental treatments of PCVBs randomize the beam in the source plane using an SLM or rotating ground-glass plate, resulting in a source correlation function of the form

$$W(\mathbf{r}_1, \mathbf{r}_2) = U^*_{nm}(\mathbf{r}_1) U_{nm}(\mathbf{r}_2) \mu(|\mathbf{r}_2 - \mathbf{r}_1|), \tag{22}$$

i.e., a beam of pure Schell-model form. It has been shown [33] that a beam-wander-model beam may be constructed by putting this Schell-model beam in the focal plane of a lens; the random angular diversity imparted on the beam by the SLM is therefore converted into a random axis displacement by the lens.

The self-healing of a beam-wander-model source can be explained readily from the mathematics. As the beam propagates, $w(z)$ increases without bound while the wander parameter δ is fixed. Therefore the ratio of $\delta/w(z)$ decreases upon propagation, and the relative wander of the beam decreases with respect to the width: it appears more coherent. This effect occurs because all realizations of the partially coherent beam are propagating parallel to each other, in contrast to the beam of Eq. (22).

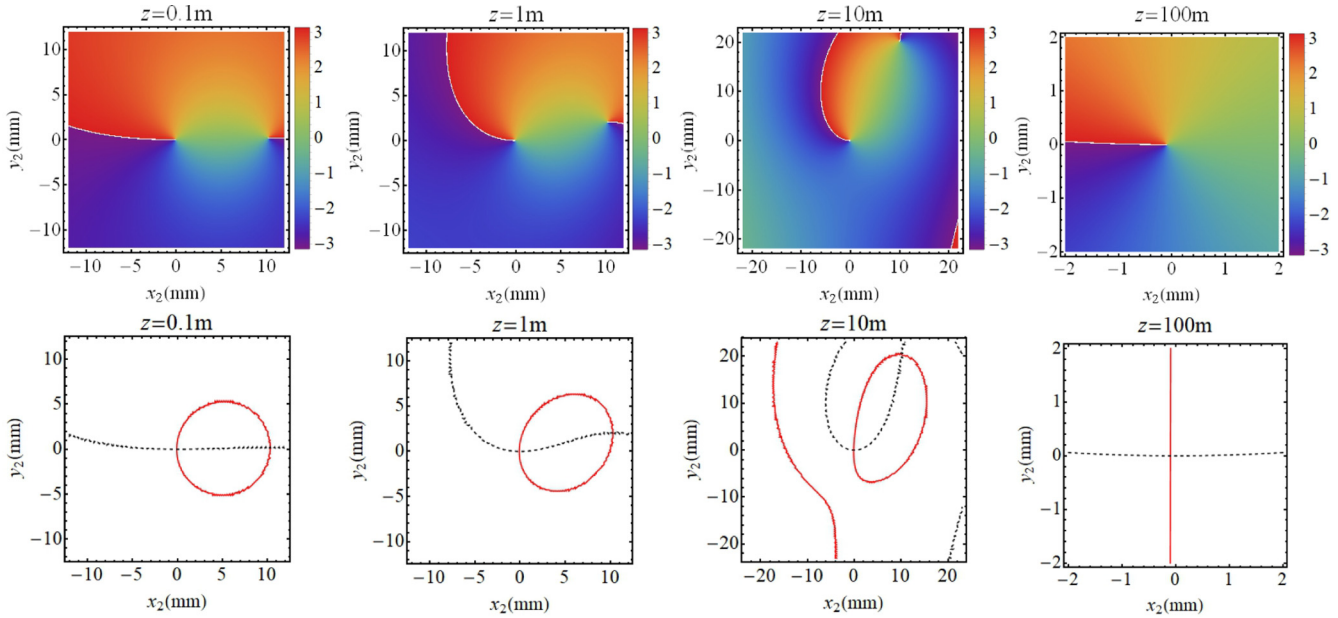

FIG. 6. Phase and corresponding zeros of the real and imaginary parts of the cross-spectral density for different propagation distances z, with $n = 0$ and $\delta = 0.1$ mm. In all images, $\mathbf{r}_1 = (0.1\text{ mm}, 0.0\text{ mm})$, $m = 1$, $w_0 = 1$ mm, and $\lambda = 632.8$ nm.

The topological reconstruction can be seen directly from Eq. (8) with some effort. As z increases, the width $w(z)$ of the beam increases without limit, and $\alpha(z) \to \delta$. We may then rewrite all terms of the form $(x \pm iy)$ in a normalized form $(x \pm iy)/(wA\delta^2)$, which accounts for the natural diffractive spreading of the beam. In doing so, it is found that the terms of the sum have an additional factor $w^{-(k_1+l_1+k_2+l_2)}$. Asymptotically, then, the sums will be dominated by the $k_1 = k_2 = l_1 = l_2 = 0$ term; overall, the cross-spectral density takes on the asymptotic limit,

$$W(\mathbf{r}_1, \mathbf{r}_2, z) \approx \pi w^{2m} D(\mathbf{r}_1, \mathbf{r}_2, z) L_n^m\left(\frac{2r_1^2}{A^2 w^2 \delta^4}\right) L_n^m\left(\frac{2r_2^2}{A^2 w^2 \delta^4}\right) \times \left(\frac{x_1 - iy_1}{Aw\delta^2}\right)^m \left(\frac{x_2 + iy_2}{Aw\delta^2}\right)^m, \tag{23}$$

which has the form of a coherent LG beam multiplied by a Gaussian Schell-model envelope, $D(\mathbf{r}_1, \mathbf{r}_2, z)$. It is noteworthy

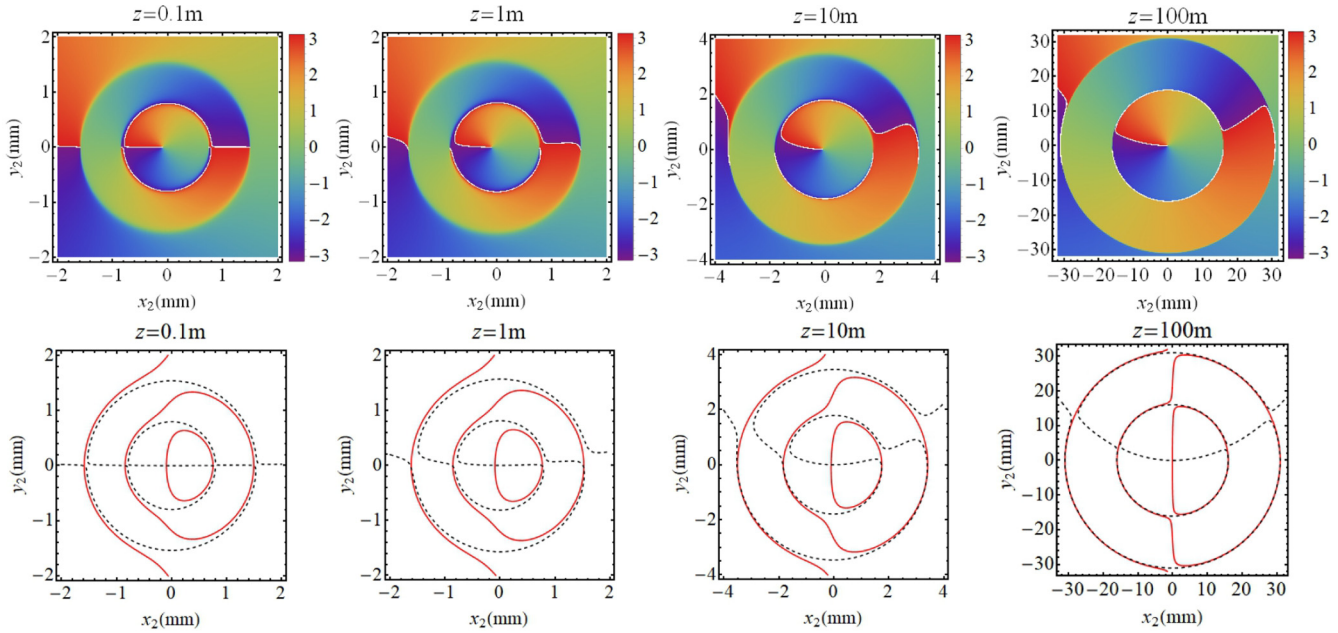

FIG. 7. Phase and corresponding zeros of the real and imaginary parts of the cross-spectral density for different propagation distances z, with $n = 2$ and $\delta = 0.1$ mm. In all images, $\mathbf{r}_1 = (0.1\text{ mm}, 0.0\text{ mm})$, $m = 1$, $w_0 = 1$ mm, and $\lambda = 632.8$ nm.

that, for this approximation to hold, the fixed observation point $\mathbf{r}_1$ must lie close to the origin.

These results show that the manner of randomization of a partially coherent vortex beam has a strong influence on its topological properties and that van Cittert–Zernike–style reconstructions can occur for some types of randomization. These observations will be explored further in future work.

V. SUMMARY AND CONCLUSIONS

This paper gives a derivation for a complete set of PCVBs, for any radial order, for any azimuthal order, and at any propagation distance, based on a beam wander model. It is, in a sense, the completion of work on partially coherent vortex beams that started long ago with the study of $n = 0$, $m = 1$ beams in Ref. [17]. It is found that the radial order of the PCVBs provides an extra degree of freedom for controlling both coherence vortices and the distribution of OAM density.

A study of radial order in PCVBs is timely, because recent research has shown that it is possible to sort photons not only by azimuthal order (OAM), but also by radial order [21,34,35]. If partial coherence is going to play a role in future optical communications employing both azimuthal and radial orders, the influence of coherence on radial modes must be understood.

As the coherence is decreased, a PCVB with a larger radial order will evolve more pairs of correlation singularities; as the beam propagates, however, the coherence vortices exhibit interesting "self-healing" characteristics, which we interpret as a van Cittert–Zernike–style evolution that depends strongly on the manner in which the beam is randomized. Our results indicate that a proper choice of randomization is essential in order to be able to resolve the vortices of partially coherent vortex beams at a detector.

The radial order also influences the properties of the orbital angular momentum. Though the total OAM is conserved, by adjusting the radial order and propagation distance, we can get different distributions of the density of the OAM. This observation can be applied to fine-tune the rotation of particles trapped in vortex beams, much like the spin and orbital angular momentum are combined for additional tuning in Ref. [8].

ACKNOWLEDGMENTS

The authors would like to acknowledge the Air Force Office of Scientific Research (AFOSR) (Grant No. FA9550-16-1-0240) and the National Natural Science Foundation of China (NSFC) (Grants No. 11474143, No. 91750201, No. 11525418, and No. 11974218).

[1] M. S. Soskin and M. V. Vasnetsov, Singular optics, in *Progress in Optics*, edited by E. Wolf, Vol. 42 (Elsevier, Amsterdam, 2001), p. 219.

[2] M. R. Dennis, K. O'Holleran, and M. J. Padgett, Singular optics: Optical vortices and polarization singularities, in *Progress in Optics, Vol. 53*, edited by E. Wolf (Elsevier, Amsterdam, 2009), p. 293.

[3] G. J. Gbur, *Singular Optics* (CRC Press, Boca Raton, FL, 2017).

[4] J. H. Lee, G. Foo, E. G. Johnson, and G. A. Swartzlander Jr., Experimental Verification of an Optical Vortex Coronagraph, Phys. Rev. Lett. **97**, 053901 (2006).

[5] D. Palacios, D. Rozas, and G. A. Swartzlander Jr., Observed Scattering into a Dark Optical Vortex Core, Phys. Rev. Lett. **88**, 103902 (2002).

[6] G. Gibson, J. Courtial, M. J. Padgett, M. Vasnetsov, V. Pas'ko, S. M. Barnett, and S. Franke-Arnold, Free-space information transfer using light beams carrying orbital angular momentum, Opt. Express **12**, 5448 (2004).

[7] L. Allen, M. W. Beijersbergen, R. J. C. Spreeuw, and J. P. Woerdman, Orbital angular momentum of light and the transformation of Laguerre-Gaussian laser modes, Phys. Rev. A **45**, 8185 (1992).

[8] N. B. Simpson, K. Dholakia, L. Allen, and M. J. Padgett, Mechanical equivalence of spin and orbital angular momentum of light: An optical spanner, Opt. Lett. **22**, 52 (1997).

[9] K. Ladavac and D. G. Grier, Microoptomechanical pumps assembled and driven by holographic optical vortex arrays, Opt. Express **12**, 1144 (2004).

[10] J. C. Ricklin and F. M. Davidson, Atmospheric turbulence effects on a partially coherent Gaussian beam: Implications for free-space laser communication, J. Opt. Soc. Am. A **19**, 1794 (2002).

[11] C. Zhao, Y. Cai, X. Lu, and H. T. Eyyuboğlu, Radiation force of coherent and partially coherent flat-topped beams on a rayleigh particle, Opt. Express **17**, 1753 (2009).

[12] J. Zhang, Z. Wang, B. Cheng, Q. Wang, B. Wu, X. Shen, L. Zheng, Y. Xu, and Q. Lin, Atom cooling by partially spatially coherent lasers, Phys. Rev. A **88**, 023416 (2013).

[13] G. Gbur and T. D. Visser, Coherence vortices in partially coherent beams, Opt. Commun. **222**, 117 (2003).

[14] D. M. Palacios, I. D. Maleev, A. S. Marathay, and G. A. Swartzlander Jr., Spatial Correlation Singularity of a Vortex Field, Phys. Rev. Lett. **92**, 143905 (2004).

[15] W. Wang and M. Takeda, Coherence Current, Coherence Vortex, and the Conservation Law of Coherence, Phys. Rev. Lett. **96**, 223904 (2006).

[16] C. S. D. Stahl and G. Gbur, Complete representation of a correlation singularity in a partially coherent beam, Opt. Lett. **39**, 5985 (2014).

[17] G. Gbur, T. D. Visser, and E. Wolf, 'Hidden' singularities in partially coherent fields, J. Opt. A **6**, S239 (2004).

[18] G. Gbur, Partially coherent vortex beams, in *Proceedings of SPIE, Vol. 10549*, edited by E. J. Galvez and D. L. Andrews (SPIE, Bellingham, WA, 2018).

[19] G. A. Swartzlander Jr. and R. I. Hernandez-Aranda, Optical Rankine Vortex and Anomalous Circulation of Light, Phys. Rev. Lett. **99**, 163901 (2007).

[20] C. S. D. Stahl and G. Gbur, Partially coherent vortex beams of arbitrary order, J. Opt. Soc. Am. A **34**, 1793 (2017).

[21] Y. Zhou, M. Mirhosseini, D. Fu, J. Zhao, S. M. H. Rafsanjani, A. E. Willner, and R. W. Boyd, Sorting Photons by Radial Quantum Number, Phys. Rev. Lett. **119**, 263602 (2017).

[22] Y. Yang, M. Chen, M. Mazil, A. Mourka, Y. Liu, and K. Dholakia, Effect of the radial and azimuthal mode indices

of a partially coherent vortex field upon a spatial correlation singularity, New J. Phys. **15**, 113053 (2013).

[23] E. Wolf, *Introduction to the Theory of Coherence and Polarization of Light* (Cambridge University Press, Cambridge, UK, 2007).

[24] S. M. Kim and G. Gbur, Angular momentum conservation in partially coherent wave fields, Phys. Rev. A **86**, 043814 (2012).

[25] A. T. O'Neil, I. MacVicar, L. Allen, and M. J. Padgett, Intrinsic and Extrinsic Nature of the Orbital Angular Momentum of a Light Beam, Phys. Rev. Lett. **88**, 053601 (2002).

[26] M. Berry, Paraxial beams of spinning light, Proc. SPIE **3487**, 6 (1998).

[27] G. Gbur and G. A. Swartzlander Jr., Complete transverse representation of a correlation singularity of a partially coherent field, J. Opt. Soc. Am. B **25**, 1422 (2008).

[28] G. Gbur, T. D. Visser, and E. Wolf, Complete destructive interference of partially coherent fields, Opt. Commun. **239**, 15 (2004).

[29] G. Gbur and R. K. Tyson, Vortex beam propagation through atmospheric turbulence and topological charge conservation, J. Opt. Soc. Am. A **25**, 225 (2008).

[30] M. V. Vasnetsov, I. G. Marienko, and M. S. Soskin, Self-reconstruction of an optica vortex, JETP Lett. **71**, 130 (2000).

[31] Y. Zhang, M. Tang, and C. Tao, Partially coherent beams, propagation in a turbulent atmosphere, Chinese Opt. Lett. **3**, 559 (2005).

[32] T. Wang, J. Pu, and Z. Chen, Propagation of partially coherent vortex beams in a turbulence atmosphere, Opt. Eng. **47**, 036002 (2008).

[33] Y. Gu and G. Gbur, Topological reactions of optical correlation vortices, Opt. Commun. **282**, 709 (2009).

[34] X. Gu, M. Krenn, M. Erhard, and A. Zeilinger, Gouy Phase Radial Mode Sorter for Light: Concepts and Experiments, Phys. Rev. Lett. **120**, 103601 (2018).

[35] D. Fu, Y. Zhou, R. Qi, S. Oliver, Y. Wang, S. M. H. Rafsanjani, J. Zhao, M. Mirhosseini, Z. Shi, P. Zhang, and R. W. Boyd, Realization of a scalable Laguerre-Gaussian mode sorter based on a robust radial mode sorter, Opt. Express **26**, 33057 (2018).